28th AIAA/CEAS Aeroacoustics 2022 Conference, 14-17 June 2022, Southampton, UK.
DOI: 10.2514/6.2022-2873

Installed jet noise reduction using a zigzag vortex generator nozzle

Anderson R. Proença*†
School of Aerospace, Transport and Manufacturing, Cranfield University, Cranfield, MK43 0AL, UK
Institute of Sound and Vibration Research, University of Southampton, Southampton, Hampshire, SO17 1BJ, UK

Jack L. T. Lawrence‡
Institute of Sound and Vibration Research, University of Southampton, Southampton, SO17 1BJ, UK

In this paper, an experimental investigation into a vortex generator ring is performed to establish its potential as a noise reduction technology for next generation of closely coupled engine-airframe aircraft. A zigzag ring was 3D-printed onto the internal surface of a round, single-stream nozzle upstream of the nozzle exit plane. Isolated and installed jet configurations were studied under static and in-flight ambient flow conditions. Unsteady pressure measurements were performed using both a linear far-field microphone array and an azimuthal near-field microphone array. Unsteady velocity data at the jet nozzle exit were acquired via hot-wire anemometry. Far-field acoustic data show that the lip treatment produces a 1 dB overall sound pressure level reduction on the jet mixing noise source. The maximum benefit for this particular noise source occurs at low jet polar angles. A greater noise reduction, in excess of 3 dB, is observed for the installed configuration, where the maximum benefit is seen at forward arc polar angles. The presence of forward flight slightly reduces the overall noise advantage provided by the vortex generator. The unsteady velocity data suggest that the zigzag ring does not alter the aerodynamic performance of the nozzle significantly, but further investigation into potential thrust penalties is necessary.

I. Nomenclature

a, b, c, d	=	dimensions used to define the zigzag ring, mm
b	=	frequency bandwidth, Hz
c	=	aerofoil chord length, mm
D	=	nozzle exit diameter, mm
f	=	frequency, s^{-1}
h	=	radial distance between nozzle centreline and aerofoil trailing edge, mm
l	=	axial distance between nozzle exit and aerofoil trailing edge, mm
m	=	mass, kg
M	=	acoustic Mach number
P	=	pressure, Pa
St	=	Strouhal number
T	=	temperature, K
T	=	thrust, N
$\mathbf{U}(U, V, W)$	=	jet local velocity, m s^{-1}
$\boldsymbol{x}(x, y, z)$	=	Cartesian coordinate system
$\boldsymbol{z}(r, \theta, z)$	=	cylindrical polar coordinate system
α	=	aerofoil angle of attack, degrees
β	=	jet spreading angle, degrees
γ	=	coherence function

*Research Fellow in Experimental Aerodynamics, Applied Aerodynamics Group, Cranfield University, AIAA Member.
†Visiting Fellow, Acoustics Group, University of Southampton
‡Senior Research Fellow in Experimental Aeroacoustics, ISVR, University of Southampton, AIAA Member.

Published by AIAA. This is the Author Accepted Manuscript issued with: Creative Commons Attribution Non-Commercial License (CC:BY:NC 4.0).
The final published version (version of record) is available online at DOI:10.2514/6.2022-2873. Please refer to any applicable publisher terms of use.

ρ = density, kg m^{-3}
ϕ = far-field azimuthal angle, $^\circ$
θ = far-field polar angle, $^\circ$

Subscripts and superscripts
$\square_0$ = total properties of a thermodynamic variable
$\square_{amb}$ = ambient properties of a thermodynamic variable
$\square_f$ = properties at the flight nozzle exit
$\square_j$ = properties at the jet nozzle exit
$\dot{\square}$ = rate of change of a property
$\overline{\square}$ = mean value of a property

II. Introduction

The exhaust jet noise produced by modern turbofan engines is a dominant noise source during the takeoff of most commercial aircraft. While substantial jet mixing noise reduction has been achieved over the years, the perceived jet noise for the next generation of turbofan engines powering twin-aisle aircraft is expected to be produced mostly due to jet-surface interaction (JSI) effects. This is a consequence of the ever-increasing engine bypass ratio, and therefore engine nacelle diameter, which results in a high-speed jet discharged close to the wing surface and high-lift devices. The scattering of the jet's hydrodynamic near pressure field by various surface discontinuities (e.g., the flap trailing edge) produces a significant low-frequency augmentation of the far-field noise [1]. Thus, reducing the physical mechanisms responsible for JSI noise generation is of high priority to aircraft and turbofan engine manufacturers.

Several investigations into the use of vortex generators to reduce subsonic jet mixing noise have been conducted in the past [2, 3]. Regarding jet mixing noise, Meyer and colleagues studied several enhanced mixing devices [4]. In their investigation, a zigzag-shaped ring glued to the internal nozzle surface was seen to provide the largest noise reduction in the acoustic far field. Overall sound pressure level (OASPL) reductions of up to 2 dB, compared to the untreated baseline nozzle, were observed. More recently, Câmara et al. studied the far-field and flow-field changes due to a zigzag tape [5]. Their thin zigzag tape had a maximum thickness of 1% of the nozzle diameter. Velocity data measured at the nozzle exit suggested that the jet mixing noise benefit was still significant even when corrected for thrust.

Nonetheless, detailed information regarding the boundary layer properties at the exit plane of modified nozzles is currently lacking in the literature. It is likely that the acoustic benefits observed with such devices are strongly sensitive to the nozzle boundary layer type and thickness compared to the size of the vortex generation device. Additionally, a rigorous investigation into the thrust penalty is essential before such a technology can be integrated onto a full-scale aircraft.

Another point to consider is that the effectiveness of the zigzag vortex generator on reducing the JSI source does not necessarily follow the observations for jet mixing noise. The incident pressure field on the wing surface, especially along the span of the trailing edge, is accountable for the increase in low-frequency noise [6–8]. The spanwise coherence of the hydrodynamic pressure field provides an indication of the magnitude of the sound pressure level in the jet far field, while the streamwise coherence dictates the width of the JSI 'hump' [9]. Thus, the presence of the zigzag ring is expected to alter the two jet noise source mechanisms differently.

In this work, previous investigations presented in the literature [4, 5] are extended, firstly, by studying the impact of a zigzag-shaped vortex generator on the JSI noise source. Secondly, an analysis of the azimuthal structure of the jet near pressure field is presented. Thirdly, the effects of forward flight are discussed using data from the Doak Flight Jet Rig, at the University of Southampton. Finally, a preliminary investigation into the effect on thrust is presented.

III. Experiments and Definitions

The experimental campaign was performed using the Flight-Jet Rig (FJR) in the anechoic Doak Laboratory, at the University of Southampton. Firstly, in this section, the experimental facility is introduced. This is followed by the definition of the zigzag ring mounted close to the nozzle exit plane. Details of the instrumentation used for controlling the rig and recording the relevant data are then presented.

A. Experimental Facility

The Doak Laboratory comprises an anechoic chamber that is fully anechoic above 300 Hz, with dimensions approximately equal to 15m-long, 7m-wide and 5m-high. The recently commissioned FJR consists of two separate air supply systems that allow forward flight simulation of single-stream, subsonic and supersonic jet flows. The primary 'core' jet flow is supplied by a high-pressure compressor-reservoir system which delivers up to 2 MPa of inlet pressure. The secondary 'flight' jet flow is supplied by a 1.1 pressure ratio fan. The 300mm-diameter flight nozzle can produce flow velocities up to Mach $M_f = 0.33$. Further information about the Doak Laboratory and FJR can be found in references [10, 11].

A rectangular wing model (profile NACA 4415) was mounted below the jet nozzle to investigate jet-surface interaction effects. The wing model has a span of 600 mm, and chord of 150 mm. The wing trailing edge was set at a radial distance from the jet geometric centreline equal to $h = 0.6D_j$, and at an axial distance from the nozzle exit plane equal to $l = 3D_j$. The wing incidence, defined as the angle between the jet centreline and wing chord, was set to $\alpha = 4°$.

Three experiments were carried out in this work. Firstly, far-field acoustic measurements were performed using a linear 'flyover' array mounted on the ceiling of the chamber (see Fig. 1(a)). This was used for both the isolated and installed jet configurations, which were tested both under static and in-flight ambient flow conditions. Secondly, the hydrodynamic near pressure field of the isolated, static jet was investigated using an azimuthal array of eight equally-spaced microphones (Fig. 1(b)). Finally, the unsteady velocity field at the jet nozzle exit was recorded using hot-wire anemometry (Fig. 1(c)).

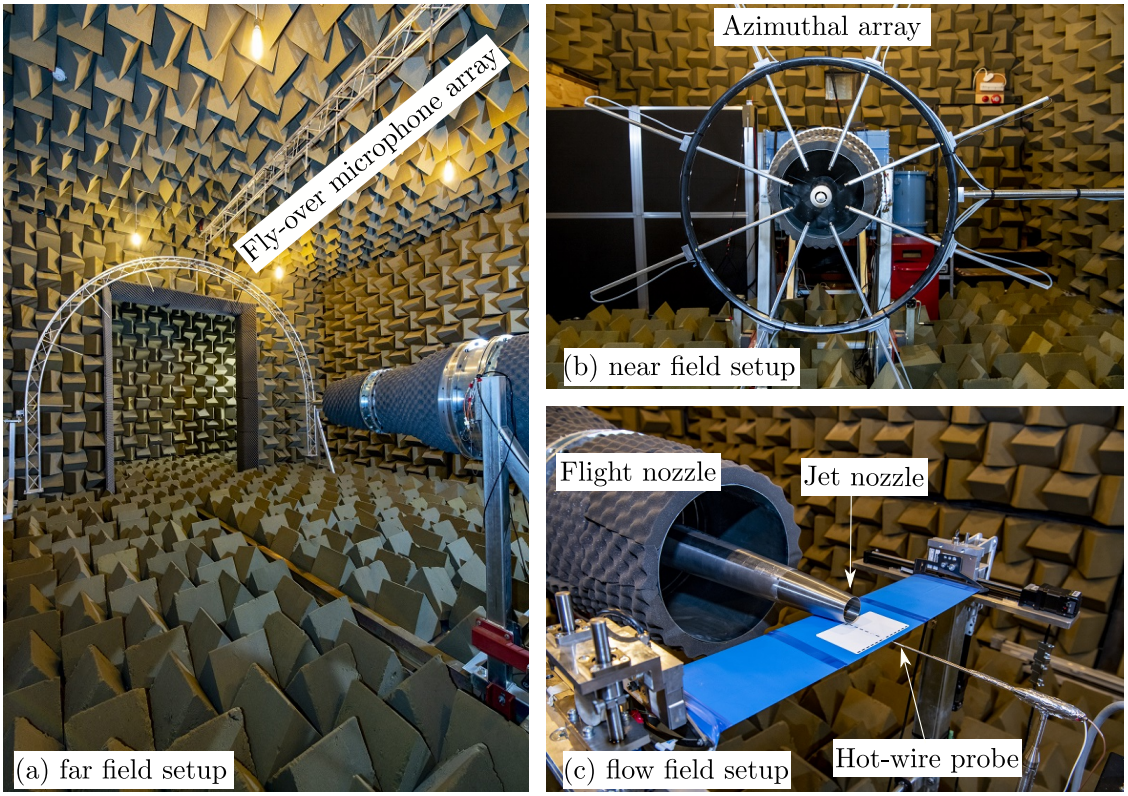


Fig. 1 The Flight Jet Rig in the Doak Laboratory, at the University of Southampton

B. Lip treatment

The passive treatment used in this work consisted of a zigzag ring mounted on the internal surface of the jet nozzle upstream of the nozzle exit plane. Fig. 2 shows a schematic of the baseline nozzle and the zigzag geometry. To avoid issues attaching a tape to the nozzle, as described in previous investigations [4, 5], the entire nozzle geometry was 3-D printed.

The zigzag geometry was designed based on far-field acoustic results from previous research [4, 5]. The dimensions

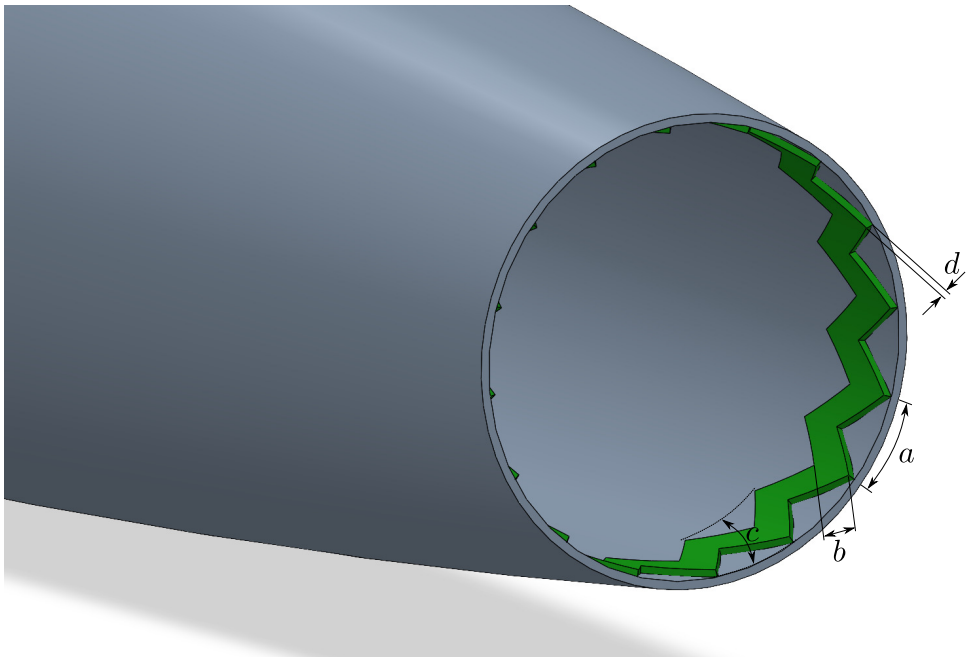


Fig. 2 Schematic showing the zigzag lip treatment used in this work

of the zigzag were normalised by the baseline round jet nozzle internal diameter to maintain consistency with other studies. The angle formed between each serration was 60°, and the lengths indicated in Fig. 2 were $a = 0.225D_j$, $b = 0.08D_j$, $c = 0.33D_j$, and $d = 0.016D_j$.

C. Instrumentation

The rig flow was controlled using in-flow pressure and temperature sensors, mounted along the rig, and ambient chamber sensors. Corrections were applied to the raw data to account for changes in relative humidity and chamber temperature throughout the tests.

Unsteady pressure data waere recorded using 1/4" B&K condenser microphones. Ten microphones were mounted in the far-field linear flyover array (i.e. $\phi = 0°$) for observer polar angles over the range $40° \leq \theta \leq 130°$, at approximately 10° intervals. Eight microphones were assembled in the near-field azimuthal array (see Fig. 1) at $\Delta\phi = 45°$ intervals. Additionally, data from wall pressure transducers flush-mounted to the wing surface were recorded for the installed configurations.

Unsteady velocity data were obtained using a Constant Temperature Anemometry (CTA) hot-wire system. Single, miniature Dantec 55P01 hot-wire probes were used to study the changes in the boundary layer properties at the nozzle exit. Measurements of the jet plume were not performed due to time constraints.

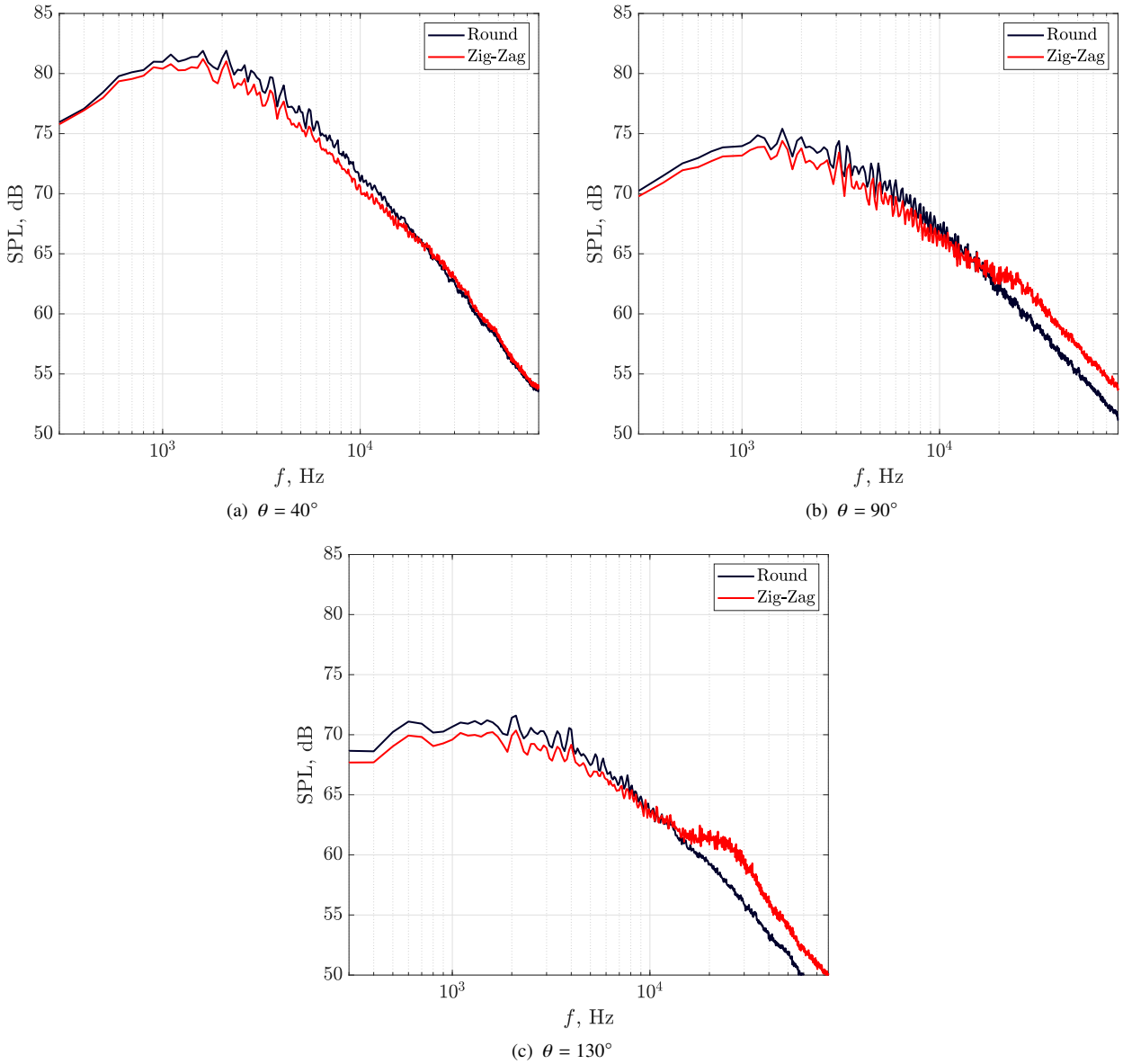
IV. Far-Field Acoustic Pressure Results

A summary of the key results obtained from the ten microphones mounted on the far-field linear microphone array is presented in this section. Trends observed in the forward and reward polar observer arcs were seen to be consistent. Thus, the plots presented below illustrate the spectra measured at $\theta = 40°$, $\theta = 90°$, and $\theta = 130°$. Additionally, the jet acoustic Mach number chosen to be presented here is equal to $M_j = 0.6$. No strong dependence on jet exit velocity was observed, apart from the expected dominance of either the jet mixing or jet-surface interaction noise sources at high- and low-subsonic speeds, respectively.

Firstly, in Sect. IV.A, the discussion is presented for the isolated jet configurations (i.e., the jet mixing noise source). Then, Sections IV.B and IV.C present the main findings for the jet-surface installation noise under static and in-flight conditions. All far-field data presented below has been corrected for distance, microphone incidence, and atmospheric attenuation. Further details of the post-processing procedure for the acoustic data used in the paper can be found in Appendix A.

A. Static jet mixing noise

Fig. 3 displays a comparison between the sound pressure level (SPL) spectra obtained for the round baseline nozzle and the nozzle treated with the zigzag vortex generator geometry. The SPL was obtained from the power spectral density estimate of the pressure signal, computed using Welch's method. The PSD values were then multiplied by the bandwidth (b = 100 Hz) and referenced to 20μPa. The overall sound pressure level was obtained by summing the energy between 300 and 50kHz. At an acoustic Mach number of 0.6, this equated to a Strouhal number range of between ... and ....



(a) $\theta = 40°$ (b) $\theta = 90°$

(c) $\theta = 130°$

Fig. 3 Isolated jet configuration sample SPL results. Nozzle with lip treatment (red) and untreated baseline (black) are shown. Jet acoustic Mach number is equal to 0.6

The trend shown in Fig. 3 agrees well with what has been presented previously in the literature. At low polar angles, a slight low-frequency benefit due to the zigzag ring is seen. At higher observer polar angles, a greater low-frequency reduction is balanced by a high-frequency penalty. Contrary to previous research, however, a maximum of 1 dB reduction is observed for the jet mixing noise, rather than 2-3 dB seen in previous works [4, 5]. The author's suspect that the differences in the boundary layer properties at the nozzle exit for each rig will explain this, but further research is required to confirm this hypothesis.

A similar analysis is presented in the next section, where the static installed jet noise is considered.

B. Static jet-surface interaction noise

Sample spectra for installed configurations are depicted in Fig. 4. Regarding low-frequency and high-frequency behaviour, the JSI noise follows a similar trend as seen for the jet mixing noise data: 1) a reduction of the low-frequency spectral components at all observer locations studied, and 2) an increase at high frequency at observer polar angles larger than $\theta = 50°$.

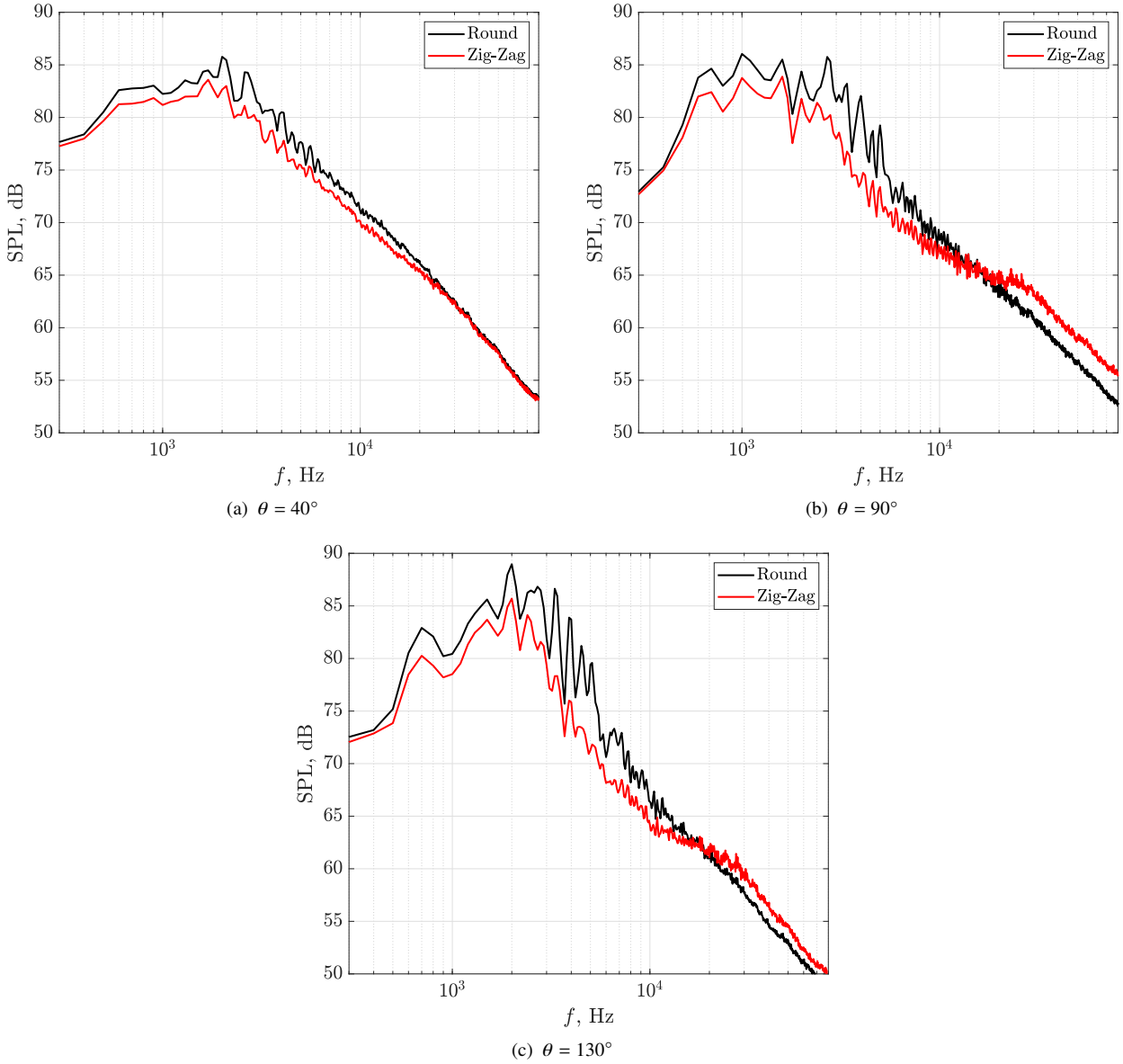


Fig. 4 Installed jet sample SPL spectra. Nozzle with lip treatment (red) and untreated baseline (black) are shown. Jet acoustic Mach number is equal to 0.6

There are two striking differences between the data presented in figures 3 and 4. Firstly, the high-frequency increase due to the presence of the zigzag ring is seen to be stronger than for the isolated jet. The moderate and high-frequency energy from the installed jet configurations is dominated by the wing-reflected jet mixing noise. The hypothesis here is that the zigzag ring naturally shifts the spectral energy from low to high-frequency structures, affecting the components

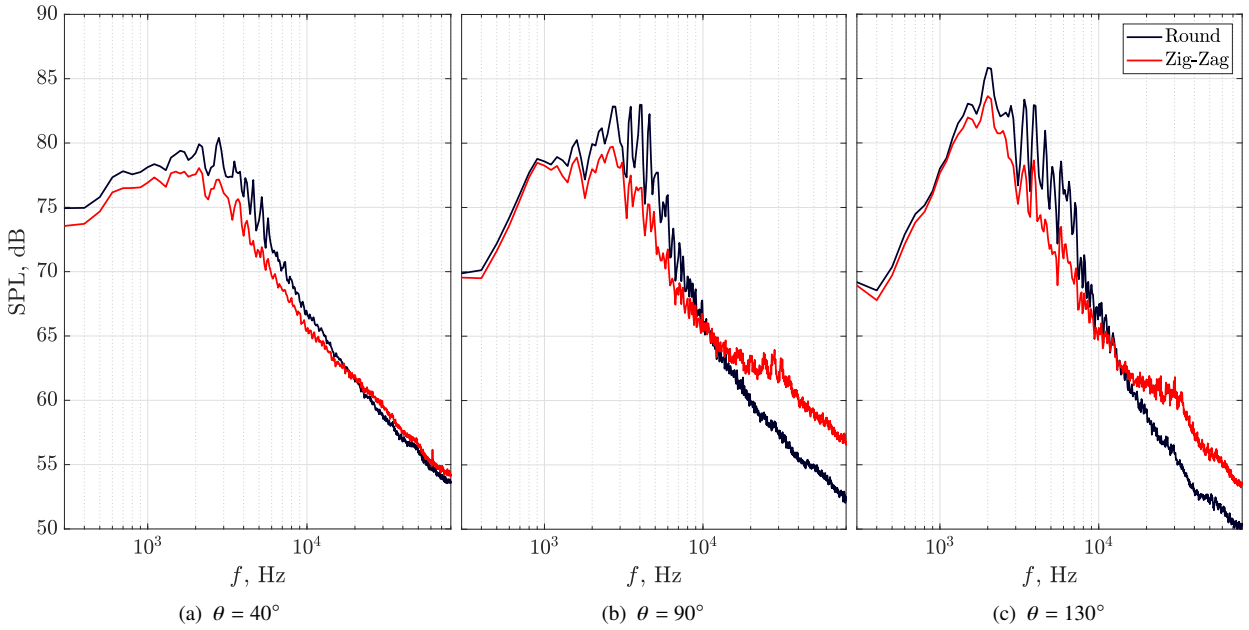
which are then reflected by the rigid structure.

The other key difference between the jet mixing noise and JSI noise effects regards the low-frequency reduction provided by the zigzag vortex generator. At all observer locations, the zigzag nozzle is seen to be more effective at reducing the JSI noise compared to jet mixing noise in that same frequency range. At this point in time, the authors believe that the zigzag ring modifies not only the boundary layer properties at the nozzle exit, but also the development of the instability that grows within the jet shear layer.

Both the reduced high-frequency penalty and the increased low-frequency reduction suggests there exists a significant potential for JSI noise reduction. In light of the results discussed in sub-sections IV.A and IV.B, several lines of research were identified. The followings sections present a preliminary stage of an on-going investigation into forward flight-effects, hydrodynamic pressure field modification, and the aerodynamic penalty associated with such a zigzag ring treatment.

C. Forward flight effects

In-flight tests were performed only for the installed jet configuration. These data are used to investigate the potential benefit of zigzag rings in more realistic conditions (e.g., a commercial aircraft during takeoff). Forward flight co-flows reduce the mixing between the jet and the ambient flows, which results in a 'stretching' of the jet plume. As expected, this fact serves to reduce the JSI source strength compared to the static case and, thus, reduces the degree of noise attenuation provided by the vortex generator. In-flight test data at the three subsonic jet acoustic Mach numbers and three flight-stream velocities were analysed. Following the template used in the previous two graphs, Fig. 5 displays the SPL spectra for both nozzle configurations at $M_j = 0.6$, at three observer polar angles.



(a) $\theta = 40°$ (b) $\theta = 90°$ (c) $\theta = 130°$

Fig. 5 Installed jet in-flight SPL results. Jet acoustic Mach number is equal to 0.6, flight-stream Mach number 0.1

Both the low-frequency and high-frequency trends are consistent with the data discussed in the previous two sub-sections. Interestingly, the high-frequency penalty introduced by the zigzag treatment is exacerbated in flight. Although the JSI hump dominates that high-frequency penalty region by more than a decade, the low-frequency reduction was also seen to decrease with flight, especially at high polar angles.

In summary, results discussed in this Section suggest that a promising amount of far-field JSI noise reduction can be achieved using such a lip treatment. Table 1 shows the overall sound pressure level obtained from integration of the data displayed in figures 3, 4, and 5. The ΔOASPL values are obtained simply by subtracting the treated nozzle data from the round, untreated baseline level.

In Sec. V, the near-field pressure results are interrogated to help pinpoint the mechanism behind the noise reductions

Table 1 Overall sound pressure level reduction for the zigzag nozzle compared to the baseline nozzle (dB

θ	isolated	installed	flight
40°	-1.0	-1.9	-1.71
90°	-0.5	-2.6	-2.11
130°	-0.2	-3.6	-2.33

observed for both the jet mixing and the jet-surface interaction noise sources. Then, in Sec. VI, the streamwise velocity profile in the nozzle exit boundary layer is used to quantify the aerodynamic penalty introduced by the zigzag ring.

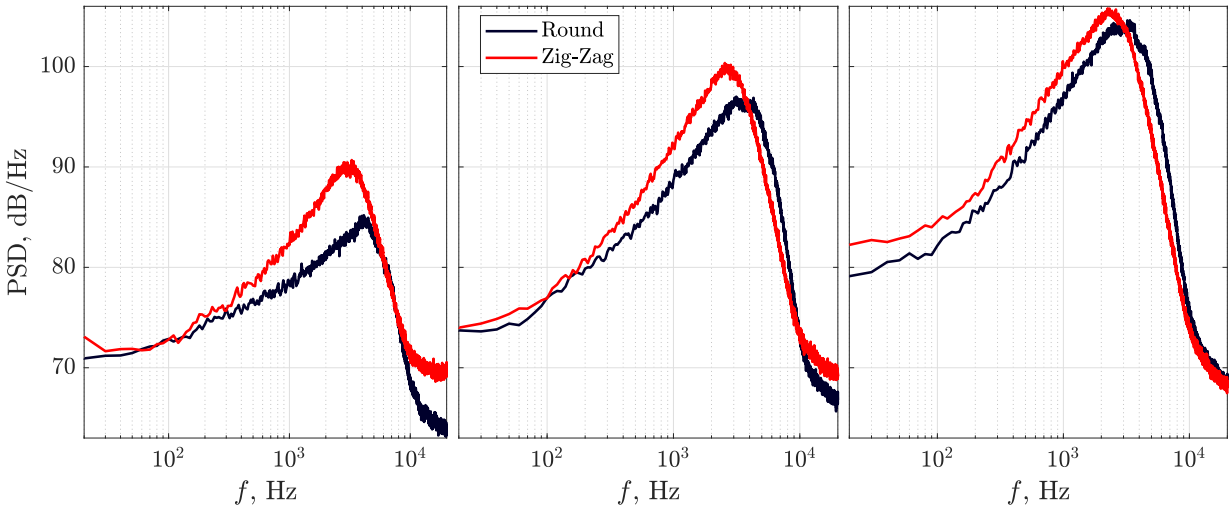
V. Near-Field Hydrodynamic Pressure Results

The azimuthal near-field array data were used to investigate changes in both the pressure autospectra and the azimuthal modal structure of the isolated zigzag nozzle. These two properties are discussed in the following sub-sections.

A. Power spectral density

In view of the far-field data presented in Sect. IV, near-field tests were conducted at a jet acoustic Mach number of 0.6 under static ambient flow conditions. Minor differences in amplitude (<2 dB) were observed across the eight near-field microphones in the low-frequency hydrodynamic pressure part of the spectra. These differences were due to the maximum microphone position accuracy achievable with the array hardware. Such positioning errors do not, however, affect the comparison between nozzle builds.

The main differences observed in the near pressure field of the baseline and zigzag nozzles were a function of both radial and axial microphone location. Compared to the baseline nozzle, the zigzag nozzle generated more hydrodynamic energy close to the nozzle exit. In Figure 6, the PSD levels measured at three axial locations of both nozzles are illustrated. The data displayed were measured at a constant radius of $r/D_j = 0.8$. As expected, the general low-frequency hydrodynamic PSD energy produced by both jets increases with increasing axial distance as the shear layer instabilities grow and as the edge of the shear layer moves closer to the microphones.



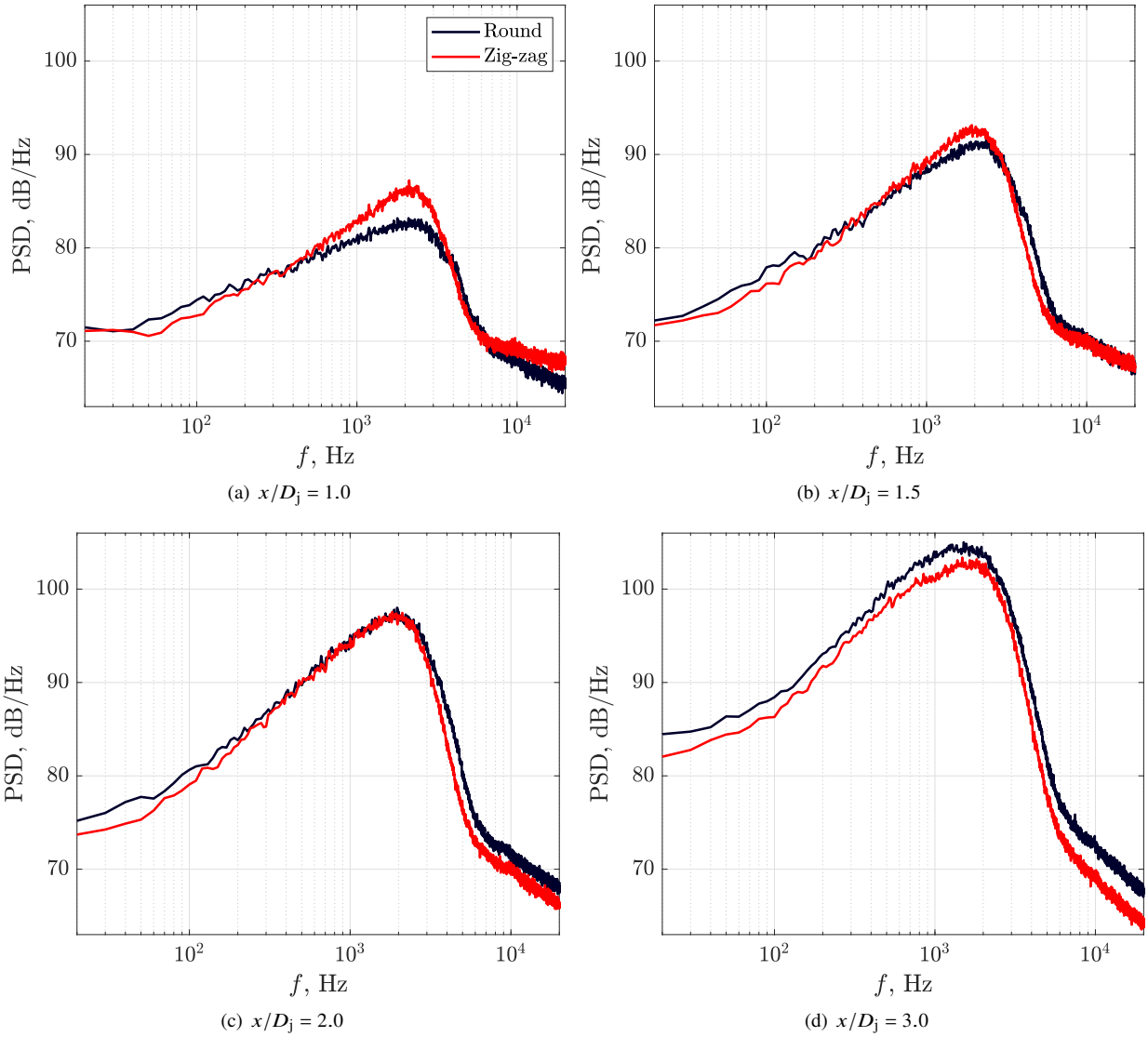
(a) $x/D_j = 0.5$ (b) $x/D_j = 1.0$ (c) $x/D_j = 1.5$

Fig. 6 Near-field PSD data at three axial locations. $M_j = 0.6$, $r/D_j = 0.8$

The zigzag nozzle is seen to produce higher PSD levels at practically all frequencies compared to the baseline nozzle. Other vortex generator mechanisms, such as chevrons, have also been seen to produce a similar effect [3]. The increased mixing provided by the lip treatment serves to increase the spreading rate of the jet. Thus, the edge of the jet plume is moved closer to the microphones due to the nozzle treatment. Note that, at this radial location, $x/D_j = 1.5$

(shown in Fig. 6(c)) is the axial limit beyond which microphone flow buffeting will occur.

This increased mixing effect also induces a faster decay of the near-field strength with distance. This is key to both the jet mixing and jet-surface interaction noise source reduction mechanisms. Fig. 7 shows near-field PSD data measured at four axial locations at a radial distance of $r/D_j = 1.1$. At this radial location, the higher PSD produced by the zigzag nozzle seen at $x/D_j = 1$ quickly diminishes at axial locations further downstream. At $x/D_j = 3$, the PSD of the zigzag nozzle is lower at all frequencies compared to the baseline nozzle. This corresponds to the axial position at which the wing trailing edge is located in the installed jet test discussed in this paper.



(a) $x/D_j = 1.0$ (b) $x/D_j = 1.5$

(c) $x/D_j = 2.0$ (d) $x/D_j = 3.0$

Fig. 7 Near-field PSD data at four axial locations. $M_j = 0.6$, $r/D_j = 1.1$

The result above is critical for the current investigation. The behaviour of the hydrodynamic near-field pressure depends strongly on the specific vortex generator geometry. Thus, a trade-off between aerodynamic loss and acoustic benefit is inevitable. Furthermore, the rates at which the jet spreads and the hydrodynamic pressure field decays are of primary importance to the degree to which jet-surface interaction noise is reduced for a given wing/flap trailing edge location, as discussed in Sect. IV.B. A more complete investigation of the near-field pressure distribution and prediction is the subject of on-going work at the ISVR.

In the next section, the coherence between near-field microphone signals is briefly discussed. The aerodynamic penalty associated with the zigzag nozzle design is then explored later, in Sec. VI.

B. Near pressure field coherence

Both the rotational and irrotational hydrodynamic pressure fields of the jet are scattered by the wing trailing edge [12, 13]. The jet's streamwise coherence dictates the 'broadness' of the JSI frequency range, while the magnitude of the JSI source is driven by the spanwise coherence along the wing trailing edge. Although the current database does not include direct measurements of the wing surface pressure, insight into the surface pressure field can be obtained from analysis of the azimuthal coherence of the near pressure field of the isolated jet.

Figure 8 illustrates the coherence measured between microphone signals for the isolated baseline and zigzag nozzles. The solid lines indicate the baseline nozzle data and the dashed lines represent the zigzag nozzle data. The location of the azimuthal array chosen here is $r/D_j = 1.1$ and $x/D_j = 2.$ as the near field signal of both nozzles have similar PSD levels (see Fig. 7(c)). The microphone located at $\phi = 0$ is selected as reference. Given the axisymmetry of the isolated jet situation, the results are independent of the reference microphone selected and the circumferential direction over which the cross-power spectrum matrix is created.

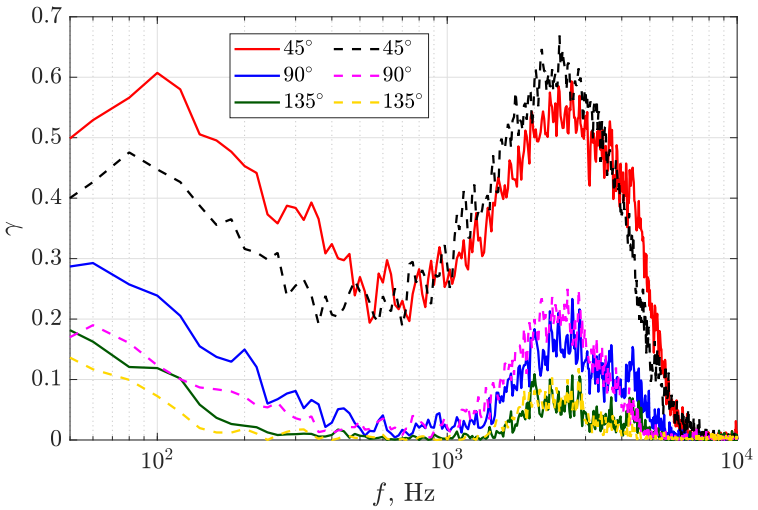


Fig. 8 Coherence results measured at $x/D_j = 2$, $r/D_j = 1.1$. Solid lines for round jet, dashed lines for zigzag jet results

Figure 8 suggests that a substantial reduction in coherence is observed at low frequencies due to the presence of the zigzag ring. This effect is reversed for frequencies higher than 1 kHz, especially for the shortest distance analysed. Similar trends were obtained for other axial locations. It is evident, therefore, that the zigzag ring not only increases the mixing rate, but also suppresses the development of large-scale structures downstream of the nozzle exit. The authors intend to pursue this research further, analysing both the azimuthal composition of the near field signal and the incident pressure on the wing surface.

VI. Aerodynamic Results

For a fixed nozzle pressure ratio, the zigzag nozzle is expected to reduce the mass flow rate compared to the baseline untreated nozzle. Hot-wire measurements were performed at the exit plane of both nozzles to estimate the discharge coefficients. The mean velocity profiles measured immediately downstream of the nozzle exit are displayed in Fig. 9. Three profiles are shown for the zigzag nozzle. For these profiles, the centre of the hot-wire probe was aligned with the 'tip' (i.e, the crest), the mid-point, and the 'end' (i.e., the trough) of the zigzag waveform when each was located at the nozzle exit.

The hot-wire probe was positioned within 1mm (i.e., $x = 0.025D_j$) downstream of the nozzle exit plane and was traversed across the y-z-plane. The position was first set by eye, before being adjusted with the assistance of pictures. Although the zigzag ring is clearly seen to modify the nozzle boundary layer profile, the boundary layer thickness was between $0.05D_j$ to $0.075D_j$ for both cases. The velocity profiles measured with respect to the three zigzag locations illustrate the azimuthal complexity of the flow.

The mass flow rate and thrust produced by the zigzag and baseline nozzles are estimated using the velocity profiles shown in Fig. 9. For both configurations, the jet flow was assumed to be axisymmetric. Before considering any form of

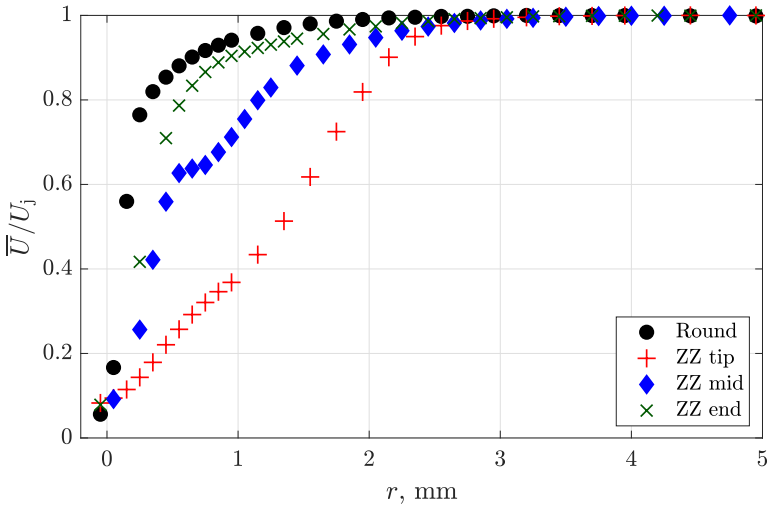


Fig. 9 Mean velocity profiles measured close to the exit plane of the baseline and zigzag nozzles

averaging for the zigzag ring data, each mean velocity profile shown in Fig. 9 was integrated over the y (or r) and θ directions (as described in the authors' previous work [14]). Table 2 displays the result of this calculation.

Table 2 Mass flow rate and thrust values computed from mean velocity profiles

	$\dot{m}$, kg/s	T, N
Round	0.308	62.032
ZZ$_{\text{tip}}$	0.307	62.018
ZZ$_{\text{mid}}$	0.309	62.264
ZZ$_{\text{end}}$	0.309	62.339

Since the boundary layer thickness measured for all situations was small, the mass flow rate and thrust values computed were expected to be close to the ideal values (i.e., $\dot{m}$ = 0.312 kg/s, and T = 63.124 N). The mass flow rate and thrust computed for two locations of the zigzag geometry are seen to be higher than the baseline, which is counter-intuitive. This occurs because the mean velocity near the centreline of the zigzag jet is 0.2 to 0.5% higher than the baseline mean velocity. Figure 10 reproduces the results shown in Fig. 9, but the range of the normalised mean velocity axis has been altered to better display a vena contracta region. Since the experimental uncertainty of the aerodynamic tests has not yet been established, it is not possible to conclude whether the zigzag ring has the real effect of diminishing the vena contracta of the jet nozzle for a fixed pressure ratio.

Another explanation regards directional effects on the single-wire probe. Cross-wires were used to perform similar tests, but the spatial resolution of these sensors is a problem. Larger round nozzles (i.e., 50 mm) will be manufactured to investigate errors due directional sensitivity of the hot-wire probes. Additional data was also acquired using an uncalibrated Venturi meter mounted upstream of the nozzle exit. Once calibrated, these data will be analysed. Nevertheless, the fact that the boundary layer remains thin is an indication that the zigzag does not produce a significantly large increase in drag.

VII. Conclusion

This paper presented an experimental investigation into the acoustic benefits of zigzag-shaped vortex generator rings for convergent, single-stream, subsonic jets. Both jet mixing noise and jet-surface interaction noise effects were studied both statically and under in-flight ambient flow conditions over a range of jet and flight Mach numbers. Jet-surface interaction noise effects were investigated using a planar rectangular wing model mounted close to the jet nozzle. Key results concerning the acoustic far field, hydrodynamic near field and the flow field close to the nozzle exit plane were all presented and discussed in the paper.

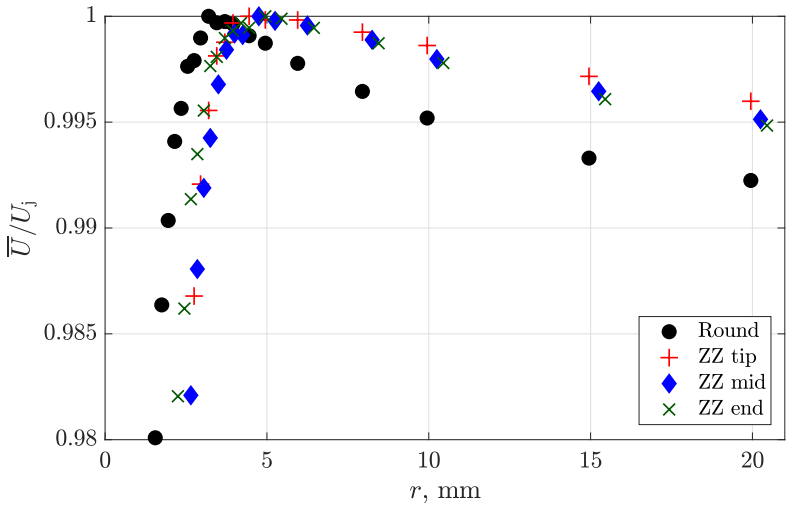


Fig. 10 Mean velocity profiles measured close to the exit plane (focused on the vena contract region)

Regarding the isolated jet mixing noise, acoustic benefits and disadvantages of the zigzag design were found to be consistent to other vortex generator devices, such as chevrons. A low-frequency noise reduction was obtained at all observer polar angles, whilst a high-frequency augmentation was present for polar angles $\theta > 50°$. A maximum overall sound pressure level reduction of 1 dB was seen at $\theta = 40°$.

More encouraging results were observed for the jet-surface interaction noise. The increased low-frequency noise attenuation resulted in overall sound pressure level reductions of up to 3.6 dB. The near pressure field data suggested that the zigzag treatment increased the mixing rate close to the nozzle as expected. The hydrodynamic pressure field was seen to decay faster compared to the baseline jet flow. Furthermore, a substantial low-frequency coherence reduction was observed from the azimuthal near-field data. This points to a breaking up of the azimuthal structure of the jet and a suppression of the instabilities that develop within the initial jet shear layer.

Finally, forward flight simulations showed that the jet-surface interaction noise reductions induced by the zigzag design were sustained at a representative takeoff situation, although the maximum OASPL benefit reduced slightly to 2.3 dB. As expected, the co-flow was seen to reduce the size of the shear layer at the wing trailing edge location, reducing the overall magnitude of the source hydrodynamic pressure field and, thus, the effect of the vortex generator. Preliminary aerodynamic results were used to investigate the aerodynamic penalty assumed due to a reduction in the nozzle discharge coefficient. While the nozzle exit boundary layer was seen to be very thin for both nozzles, no strong conclusion could be provided at this stage. Future flow field measurements on larger scale vortex generator nozzles are planned to provide clarity on the relationship between nozzle pressure ratio and thrust.

Appendix

A. Far-field corrections

Both the near-field and far-field microphone signals were acquired for 10 seconds, filtered using a 20 Hz high-pass filter and then amplified using B&K Type 2690 Nexus amplifiers. The time signals were corrected for amplifier gain and microphone capsule calibration sensitivity before being transformed into the frequency domain using a Hamming window-averaged Fast Fourier Transform, following Welch's overlapped segment-averaging spectral estimation method.

The far-field acoustic spectra were then corrected for electronic background noise, atmospheric absorption, microphone incidence angle and microphone distance (assuming spherical wave propagation) to yield the final free-field, 1m-lossless values. The static jet near-field spectra were only corrected for electronic background noise. The in-flight jet far-field data were further corrected by subtracting the 'flight background' (i.e., matched core and flight jet velocity) far-field noise levels in order to remove any extraneous aerodynamic noise generated either by the mixing noise from the flight jet or noise produced by the flight jet flow passing around the central core jet pipework and aerofoil. The spectral data plotted in the paper are reported as sound pressure levels (ref. 20 μPa) with a frequency band resolution of 100 Hz for display clarity.

References

[1] Head, R., and Fisher, M., *Jet/surface interaction noise - Analysis of farfield low frequency augmentations of jet noise due to the presence of a solid shield*, 1976. https://doi.org/10.2514/6.1976-502, URL https://arc.aiaa.org/doi/abs/10.2514/6.1976-502.

[2] Samimy, M., Zaman, K. B. M. Q., and Reeder, M. F., "Effect of tabs on the flow and noise field of an axisymmetric jet," *AIAA Journal*, Vol. 31, No. 4, 1993, pp. 609–619. https://doi.org/10.2514/3.11594, URL https://doi.org/10.2514/3.11594.

[3] Zaman, K., Bridges, J., and Huff, D., "Evolution from 'Tabs' to 'Chevron Technology' - A Review," *International Journal of Aeroacoustics*, Vol. 10, No. 5-6, 2011, pp. 685–709. https://doi.org/10.1260/1475-472X.10.5-6.685, URL https://doi.org/10.1260/1475-472X.10.5-6.685.

[4] Meyer, R., Kuo, C.-W., and McLaughlin, D. K., "Reduction of Subsonic Jet Noise by Passive Flow Control Devices," *19th AIAA/CEAS Aeroacoustics Conference*, 2013. https://doi.org/10.2514/6.2013-2147, URL https://arc.aiaa.org/doi/abs/10.2514/6.2013-2147.

[5] Câmara, F. A., Rosa, V. H., and Deschamps, C. J., "Reduction of Jet Mixing Noise with a Zigzag-Shaped Vortex Generator," *AIAA AVIATION 2020 FORUM*, 2020. https://doi.org/10.2514/6.2020-2574, URL https://arc.aiaa.org/doi/abs/10.2514/6.2020-2574.

[6] Vera, J. V., Lawrence, J., Kingan, M., Self, R., and Sinayoko, S., *Hydrodynamic pressure field propagation model for the prediction of the far-field sound produced by jet-wing interaction*, 2016. https://doi.org/10.2514/6.2016-2859, URL https://arc.aiaa.org/doi/abs/10.2514/6.2016-2859.

[7] Lyu, B., Dowling, A. P., and Naqavi, I., "Prediction of installed jet noise," *Journal of Fluid Mechanics*, Vol. 811, 2017, p. 234–268. https://doi.org/10.1017/jfm.2016.747.

[8] Faranosov, G., Belyaev, I., Kopiev, V., and Bychkov, O., "Azimuthal Structure of Low-Frequency Noise of Installed Jet," *AIAA Journal*, Vol. 57, No. 5, 2019, pp. 1885–1898. https://doi.org/10.2514/1.J057476, URL https://doi.org/10.2514/1.J057476.

[9] Meloni, S., Proença, A. R., Lawrence, J. L., and Camussi, R., "An experimental investigation into model-scale installed jet–pylon–wing noise," *Journal of Fluid Mechanics*, Vol. 929, 2021, p. A4. https://doi.org/10.1017/jfm.2021.831.

[10] Proença, A., "Aeroacoustics of isolated and installed jets under static and in-flight conditions," Ph.D. thesis, University of Southampton, March 2018. URL https://eprints.soton.ac.uk/426880/.

[11] Proença, A., Lawrence, J., and Self, R., "Experimental Investigation into the Turbulence Flowfield of In-Flight Round Jets," *AIAA Journal*, Vol. 58, No. 8, 2020, pp. 3339–3350. https://doi.org/10.2514/1.J059035, URL https://doi.org/10.2514/1.J059035.

[12] Amiet, R., "Noise due to turbulent flow past a trailing edge," *Journal of Sound and Vibration*, Vol. 47, No. 3, 1976, pp. 387–393. https://doi.org/https://doi.org/10.1016/0022-460X(76)90948-2, URL https://www.sciencedirect.com/science/article/pii/0022460X76909482.

[13] Amiet, R., "Effect of the incident surface pressure field on noise due to turbulent flow past a trailing edge," *Journal of Sound and Vibration*, Vol. 57, No. 2, 1978, pp. 305–306. https://doi.org/https://doi.org/10.1016/0022-460X(78)90588-6, URL https://www.sciencedirect.com/science/article/pii/0022460X78905886.

[14] Proença, A. R., and Lawrence, J. L. T., "Experimental Flowfield Analyses of Installed Subsonic Jet–Pylon Interaction," *AIAA Journal*, Vol. 0, No. 0, 2021, pp. 1–13. https://doi.org/10.2514/1.J060762, URL https://doi.org/10.2514/1.J060762.



https://dspace.org/

Installed jet noise reduction using a zigzag vortex generator

Proenca, Anderson R.; Lawrence, Jack

2022-06-13
American Institute of Aeronautics and Astronautics (AIAA)
https://doi.org/10.2514/6.2022-2873
Proenca A, Lawrence J. (2022) Installed jet noise reduction using a zigzag vortex generator. In: 28th AIAA/CEAS Aeroacoustics 2022 Conference, 14-17 June 2022, Southampton UK, Paper number AIAA 2022-2873

Downloaded from a DSpace repository. https://dspace.org/